III. RADIO ASTRONOMY[*]

A. HEIGHT RESOLUTION OF REMOTE SENSING OF THE ATMOSPHERIC TEMPERATURE PROFILE

1. Inversion with Noiseless Data

Radiometers at N frequencies sense the upward flux of atmospheric radiation. The measurements give the data set of brightness temperatures B_i $(i = 1, 2, \ldots, N)$, from which we wish to determine the temperature profile $T(z)$ at various heights z. We simplify the radiative transfer equation and obtain the linear transformation[1]

$$B_i = \int_{z_\ell}^{z_u} W_i(z) \, T(z) \, dz, \qquad i = 1, 2, \ldots, N. \tag{1}$$

The data kernel $W_i(z)$ is a weighting function. Its slight dependence on temperature is neglected here, and precise values of the limits of integration z_ℓ and z_u $(z_\ell < z_u)$ are irrelevant to our discussion.

Consider any linear combination of the data

$$L = \sum_i a_i B_i. \tag{2}$$

Here and elsewhere, the index of summation runs from 1 to N. The coefficients a_i will be determined by the demand on L. With a limited amount of data, we cannot expect to determine the temperature at z_o, a height level of interest. Following the method of Backus and Gilbert,[2] we combine Eqs. 1 and 2 to obtain

$$L(z_o) = \int A(z, z_o) \, T(z) \, dz \tag{3}$$

with

$$A(z, z_o) = \Sigma \, a_i(z_o) \, W_i(z). \tag{4}$$

Equation 3 suggests that we demand that $L(z_o)$ be an estimate of the average temperature around z_o. Denoting this estimate $T^*(z_o)$, we have

$$T^*(z_o) = \int A(z, z_o) \, T(z) \, dz$$

$$= \Sigma \, a_i(z_o) \, B_i. \tag{5}$$

$A(z, z_o)$ is therefore an averaging kernel that satisfies the unimodular constraint

$$\int A(z, z_o) \, dz = 1. \tag{6}$$

Note that we do not constrain A to be positive for all z.

The coefficients a_i will be determined by requiring that $A(z, z_o)$ be a function of z that is sharply peaked around z_o. Quantitatively, we seek a_i that minimize some "spread"

$$s = \int J(z, z_o) \, A(z, z_o)^2 \, dz. \tag{7}$$

There are two reasons for squaring A. First, A is possibly negative; and second, squaring A permits us to solve a_i from a set of linear equations. Here, J is some cost function, and s has the dimension of length if J has the dimension of length squared. Backus and Gilbert[2] have suggested several forms for J. In the present study we use

$$J(z, z_o) = 12 \, (z-z_o)^2. \tag{8}$$

The normalization factor 12 ensures that s = h if A is constant $(1/h)$ over the region $z = z_o \pm h/2$ and zero elsewhere.

In the mathematical manipulation procedure that follows we determine a_i in Eq. 4 by minimizing s in (7), subject to the unimodular constraint (6). The linear combination (5) then gives the estimated temperature with a spread s that is minimum according to the criterion (8).

Using -2λ as the Lagrangian multiplier, we find a_i that minimize without any constraint the quantity

$$Q = s - 2\lambda\left[\int A(z, z_o)\, dz - 1\right]. \tag{9}$$

Differentiating Q with respect to a_i and λ yields the set of linear equations

$$\underline{\underline{C}}\, \underline{a} = \lambda \underline{w}$$

$$\underline{w}^T \underline{a} = 1, \tag{10}$$

where superscript T denotes vector transpose, $\underline{a}(z_o) = (a_1 a_2 \dots a_N)^T$, $\underline{w} = (w_1 w_2 \dots w_N)^T$, $w_i = \int W_i(z)\, dz$, and $\underline{\underline{C}}$ is an $N \times N$ symmetric matrix with elements

$$c_{ij}(z_o) = \int J(z, z_o)\, W_i(z)\, W_j(z)\, dz. \tag{11}$$

If no two of the N weighting functions overlap completely, the matrix inverse $\underline{\underline{C}}^{-1}$ exists, and the set (10) can be solved for $\underline{a}$:

$$\underline{a}(z_o) = \frac{\underline{\underline{C}}^{-1}\underline{w}}{\underline{w}^T \underline{\underline{C}}^{-1}\underline{w}}. \tag{12}$$

The spread readily follows from Eq. 7,

$$s(z_o) = \underline{a}^T \underline{\underline{C}}\, \underline{a}$$

$$= 1/\underline{w}^T \underline{\underline{C}}^{-1}\underline{w}, \tag{13}$$

where s can be large on two accounts. If we define the centroid of the averaging kernel as

$$c = \int z A(z, z_o)^2\, dz / \int A(z, z_o)^2\, dz,$$

then from simple algebra

$$s = 12 \int (z-c)^2 A(z, z_o)^2\, dz + 12 (c-z_o)^2 \int A(z, z_o)^2\, dz. \tag{14}$$

The first term is large when A has significant sidelobes, while the second term is large when the centroid of A is far away from z_o.

2. Inversion with Noisy Data

When the data set of brightness temperatures is corrupted by receiver noise ΔB_i, Eq. 2 is modified to

$$L_n = \Sigma \ a_i(B_i + \Delta B_i),$$

where B_i is still defined by Eq. 1. Quantities with subscript n are affected by noise. The additive noise is assumed to have zero mean and known covariance matrix $\underline{\underline{K}}$ with elements

$$k_{ij} = \langle \Delta B_i \Delta B_j \rangle, \qquad i, j = 1, 2, \ldots, N,$$

where the angular brackets denote ensemble average.

The inferred temperature, apart from being an average around z_o, is therefore also noisy.

$$T_n^*(z_o) = \Sigma \ a_i(B_i + \Delta B_i)$$

$$= \int A(z, z_o) \ T(z) \ dz + \Sigma \ a_i \Delta B_i.$$

The estimation error has zero mean and variance

$$\sigma_n^2 = \left\langle \left(T_n^* - T^*\right)^2 \right\rangle$$

$$= \underline{a}^T \underline{\underline{K}} \, \underline{a}.$$

We now wish to infer a reliable estimate at the sacrifice of resolution. Suppose that our choice of a compromise between reliability and resolution can be linearly parametrized in the form

$$s_n(z_o, \theta) = \theta s + (1-\theta)g^2 \sigma_n^2, \qquad 0 \leqslant \theta \leqslant 1, \tag{15}$$

where s is defined by Eq. 7, g^2 is a dimensional conversion factor (a convenient choice of g^2 is $Nhw_i^2/\Sigma \ k_{ii}$), and θ is a free parameter. Equation 15 permits more emphasis on reliability and less on resolution as θ decreases from 1 to 0. Backus and Gilbert call the graph of s against $g^2\sigma_n^2$ a trade-off curve, with each point on it having associated an (n+1)-tuple $(\theta, a_1, a_2, \ldots, a_N)$. The coefficients $a_i(z_o, \theta)$ are chosen to minimize s_n, subject to the unimodular constraint (6). Proceeding as we did with noiseless data, we minimize the unconstrained quantity $Q_n = s_n - 2\lambda[\int A(z, z_o) \, dz - 1]$, and obtain

$$\underline{a} = \lambda \underline{\underline{M}}^{-1} \underline{w}, \tag{16}$$

where $\underline{\underline{M}} = \theta \underline{\underline{C}} + (1-\theta)g^2 \underline{\underline{K}}$, and $\lambda = 1/\underline{w}^T \underline{\underline{M}}^{-1} \underline{w}$.
The spread is now

$$s(z_o) = \underline{a}^T \underline{\underline{C}} \, \underline{a}$$

$$= \lambda^2 \underline{w}^T \underline{\underline{M}}^{-1} \underline{\underline{C}} \, \underline{\underline{M}}^{-1} \underline{w}. \tag{17}$$

Equation 14 still applies. Also, the error variance is

$$\sigma_n^2(z_o) = \underline{a}^T \underline{\underline{K}} \, \underline{a}$$

$$= \lambda^2 \underline{w}^T \underline{\underline{M}}^{-1} \underline{\underline{K}} \, \underline{\underline{M}}^{-1} \underline{w}.$$

When $\theta = 1$, Eqs. 16 and 17 reduce to Eqs. 12 and 13, respectively.

3. Numerical Illustration

The method described above is used to study the resolution of sensing the temperature profile with 3 microwave radiometers, as part of the Nimbus E weather satellite experiments. The frequencies centering at 53.65, 54.9, and 58.8 GHz are in the oxygen-absorption spectrum. For purposes of these calculations, the corresponding weighting functions can be well approximated by

$$W_i(z) = A_i z^{n_i} \exp(-B_i z),$$

where

$$A_i = (1 - e^{-\tau_i}) \frac{(n_i/Z_i)^{n_i+1}}{\Gamma(n_i+1)} \qquad \text{and} \quad B_i = n_i/Z_i,$$

with Γ the gamma function, Z_i the peak height of the weighting function, and n_i measuring its spatial extent. $W_i(z)$ has been normalized so that it has total area $1 - e^{-\tau_i}$, with $e^{-\tau_i}$ the total transmittance at nadir. These analytic expressions are plotted in Fig. III-1 with the values given in Table III-1. For comparison, Fig. III-1 also shows the three weighting functions calculated by using the radiosonde measurements made over Balboa, Panama, on June 3, 1966. The agreement is satisfactory.

The analytic forms of the weighting functions allow closed-form evaluation of the matrix coefficients c_{ij} in Eq. 11

$$c_{ij}(z_o) = 12 \, \Gamma(m) \frac{A_i A_j}{B_{ij}^{m+2}} \left[(B_{ij} z_o - m)^2 + m \right],$$

where $B_{ij} = B_i + B_j$, and $m = n_i + n_j + 1$ need not be an integer.

Some results are shown in Fig. III-2. The spread s is defined by a quadratic J
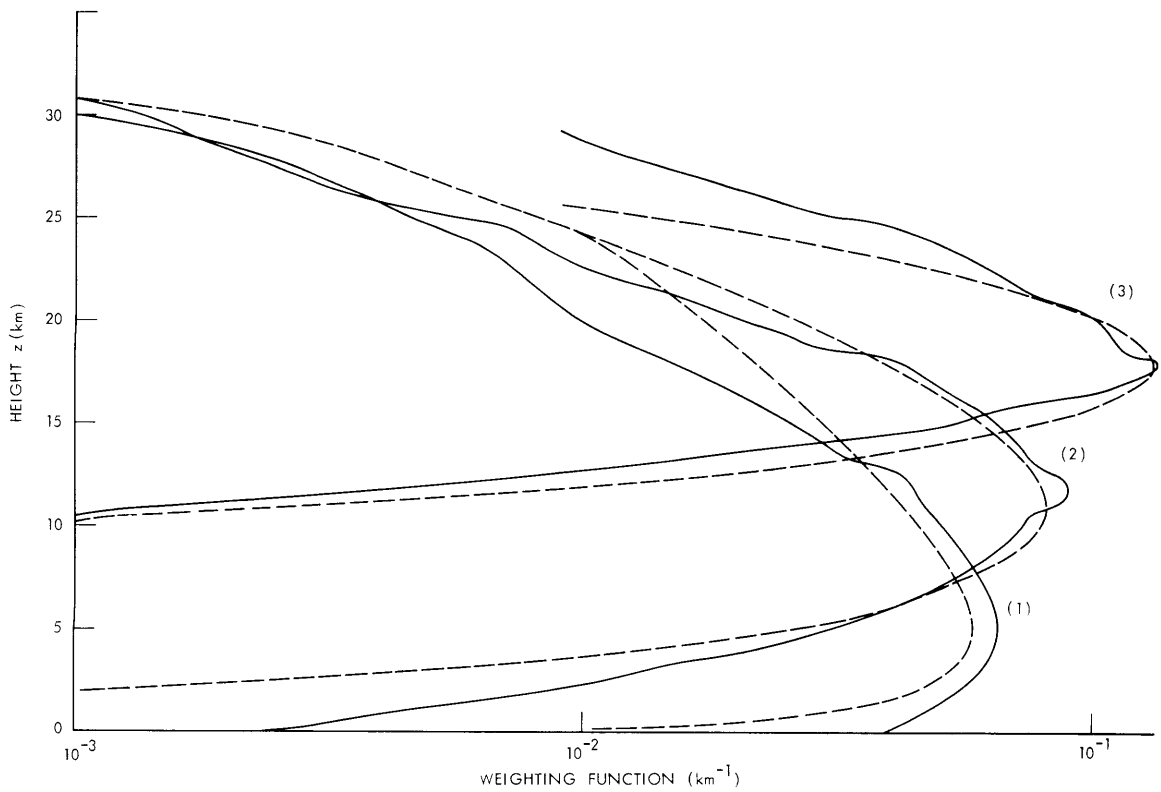
Fig. III-1. Weighting functions calculated by using radiosonde data (solid curve) and analytic approximation (dotted curve).

Table III-1. Parameters for weighting functions.

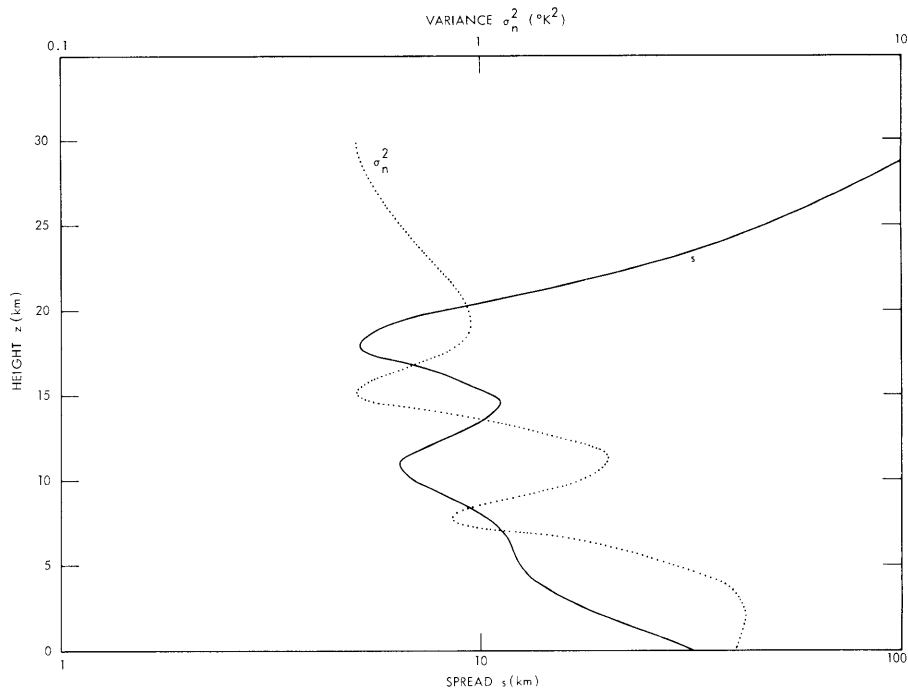| Channel i	1	2	3
Frequency (GHz)	53.65	54.9	58.8
Z_i (km)	5	11	18
n_i	0.75	5	35
$e^{-\tau_i}$	0	0	0.1

Fig. III-2. Spread and variance calculated by using analytic approximation.

Fig. III-3. Trade-off between spread and variance.
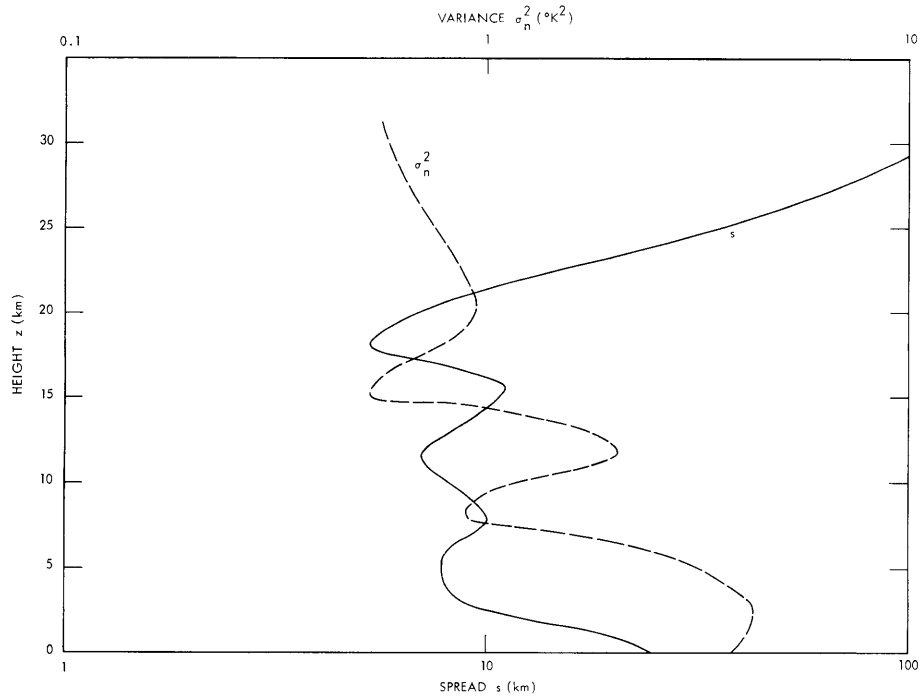
VARIANCE σ_n^2 (°K²)

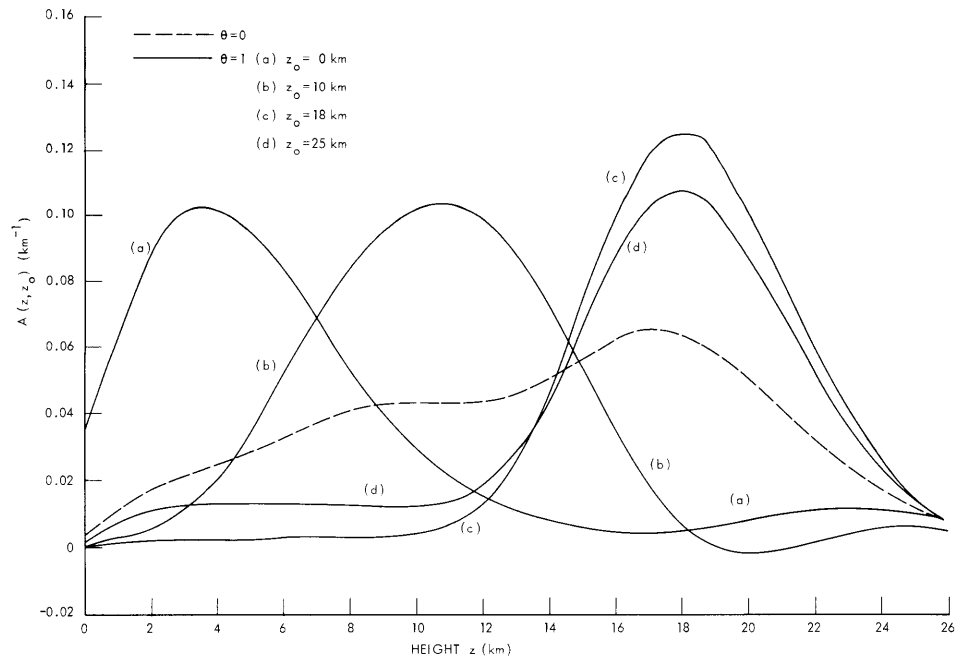Fig. III-4. Spread and variance calculated by using radiosonde data.

Fig. III-5. Averaging kernels at typical heights.

(Eq. 8) with h = 1 km. As expected, the resolution is high in regions where the weighting functions peak. In particular, the highest resolution (~5 km) occurs at the peak (~18 km above sea level) of the third weighting function, which has the least spatial span. Also plotted in Fig. III-2 is the variance σ_n^2 of the estimation error caused by 1°K rms receiver noise which is uncorrelated from one radiometer to another. Generally, σ_n^2 shows a height dependence inverse to that of s. The curves are drawn for $\theta = 1$. That is, at each level s attains its minimum value at the expense of maximum σ_n^2. For values of θ closer to 0, the graph of s will be shifted to larger values, and the graph of σ_n^2 to smaller values. The trade-off curves for 3 typical height levels are plotted in Fig. III-3. They are all concave upward, as proved by Backus and Gilbert.[2]

Using the Balboa radiosonde measurements, we integrate Eq. 11 numerically for the matrix elements and obtain the spread s and variance σ_n^2 shown in Fig. III-4. The analytic curves in Fig. III-2 predict a larger spread near the surface because the analytic approximation is smaller there than the first Balboa weighting function (Fig. III-1). Otherwise, agreement between the analytic curves and the Balboa curves is satisfactory.

Again, using the analytic approximation, we compute the averaging kernels at typical height levels (Fig. III-5). The dotted curve shows the averaging kernel at all levels when the estimator has chosen $\theta = 0$. Assuming $k_{ij} = \delta_{ij}$ (the Kronecker delta), $w_i = 1$, and $\theta = 0$, we can prove that the averaging kernel is simply the arithmetic mean of all of the weighting functions. Thus reliability is sought through equal emphasis on all radiometers, since they have the same rms noise in this calculation.

In Fig. III-5, there is an interesting feature in the solid curves for $\theta = 1$. The averaging kernel at a particular height, z_o, does not generally peak at z_o; its maximum is biased toward the peak of the third weighting function. This is demonstrated clearly for the averaging kernel at 29 km, which peaks at around 18 km because the upper levels are not spanned by weighting functions. Thus the spread (s ~ 100 km) in Figs. III-2 and III-4 is large, not so much because it has a large spatial extent or significant sidelobes (Eq. 14), but mainly because $A(z, z_o)$ does not peak around z_o.

<div align="right">R. K. L. Poon, D. H. Staelin</div>

References

1. D. H. Staelin, "Passive Remote Sensing at Microwave Wavelengths," Proc. IEEE 57, 427-439 (1969).

2. G. E. Backus and J. F. Gilbert, "Uniqueness in the Inversion of Inaccurate Gross Earth Data," Phil. Trans. Roy. Soc. London A 266, 123-192 (1970); G. E. Backus, "Inference from Inadequate and Inaccurate Data," Proc. Natl. Acad. Sci. U.S. 65, 1-7 (1970); 65, 281-287 (1970); 67, 282-289 (1970).

B. INVESTIGATION OF MICROWAVE RADIOMETRY AS A
   MEDICAL DIAGNOSTIC TECHNIQUE

1. Technique

We have begun a program to investigate the potential of the microwave radiometer as a medical diagnostic instrument for the sensing of subcutaneous temperatures in a noninvasive manner. Of the two forms of electromagnetic radiation which penetrate the human body, x ray and radio frequencies, little use has been made of radio frequencies except in the area of microwave diathermy. Largely under the impetus of radio astronomy, microwave radiometers that are capable of measuring thermal emission from the body with a sensitivity of a fraction of a degree have reached a high state of development. Since radio frequencies penetrate the body, the intensity of thermal emission is a measure of the subsurface body temperature and thus is indicative of subcutaneous conditions. Thus microwave radiometry has potential advantages as a medical diagnostic technique.

Thermal emission from the human body is the basis for infrared thermography, but, since infrared wavelengths penetrate the body very little, the results indicate only the surface temperature. Nevertheless, infrared thermography has been utilized in the study of a wide variety of medical problems.[1] One of the most publicized applications of thermography has been in the detection of malignant tumors of the breast.[2] Elevated skin temperatures of 1-3°C have been detected over many tumors. This raises the interesting question of whether or not such tumors could be detected at an earlier stage of development by sensing a subsurface temperature anomaly with a microwave radiometer. Other applications of the microwave method are suggested by analogy with infrared thermography. These include extent and degree of frostbite and burn damage, and a wide range of circulatory disorders which give rise to thermal effects.

The microwave method appears to offer some significant advantages over the infrared technique in providing body temperatures. First, and foremost, since it provides a measure of internal body temperatures, it is hoped that microwaves will provide an earlier indication of disease than infrared wavelengths. Second, for infrared thermography great care must be taken to ensure that the skin temperature of the subject is representative of the condition of the subject and not of the subject's surroundings. For example, clothing must be removed from the portion of the body under investigation, the subject must remain at rest for 10-15 minutes in a cool room of constant temperature, free of air currents, and no objects appreciably hotter or colder than the room temperature should be in the subject's line-of-sight. These are often difficult conditions to meet and they seriously limit the operational utility of infrared thermography. For the microwave method, however, the sensed temperature is an internal one and is relatively uninfluenced by external conditions. In fact, thin cloth or plastic will

appear transparent to microwaves so that all clothing need not be removed by the subject. Furthermore, no 10- or 15-minute waiting period will be required for the body to reach thermal equilibrium with its surroundings, and special temperature-controlled rooms are not needed. These advantages strongly suggest that the microwave method is well suited to mass screening of large segments of the population, if it can be shown to be of value.

A question of vital interest to the success of the microwave technique is the depth of penetration of microwave energy into the body. The penetration is typically the inverse of the absorption coefficient, a value that may fluctuate widely within the body. For example, tissue with a high water content will be relatively lossy at microwave frequencies; it will absorb strongly, so that the depth of penetration is small. Conversely, fatty tissue with relatively little water content will permit greater penetration.

In general, longer wavelengths penetrate deeper than shorter wavelengths, as might be expected. A considerable literature exists on the dielectric and conductive properties of tissue at microwave frequencies,[3-6] and one can predict with some confidence the penetration at specific frequencies. Thus a frequency of 3 GHz will penetrate dry, fatty tissue approximately 5 cm but will penetrate only ~1 cm in tissue with a high water content. Experiment shows that the microwave absorption coefficient of breast carcinoma is some five times larger than that of breast fat,[5] a circumstance which in some cases may be beneficial in the microwave method of tumor detection.

2. Current Experimental Work

Recent work has been concentrated on assembly and testing of the 3-GHz radiometer; and on development of suitable antennas. The radiometer is a comparison or Dicke-switched type, used in many microwave applications where sensitivity to small changes in input radiation power is desired. A ferrite switch alternately samples the signal port and a reference port at a rate of 15 Hz. The local-oscillator signal frequency was chosen to permit double-sideband operation of the radiometer. The broad intermediate-frequency 10-110 MHz bandwidth is as wide as was practical to obtain, in order to minimize the radiometer noise. The measured system temperature is ~700° K. Calibration is provided by an argon gas tube, attenuated to provide a noise signal of 5° K. The radiometer was assembled from available or purchased components, with the exception of the ferrite switch driver, which was in-house designed and built.

Much work has centered on antenna design and development because it is the antenna which must successfully couple the radiation from the tissue into the radiometer. The initial design is a dielectric-filled rectangular waveguide, with one end open and flanged. The plane surface of the end of the filled waveguide constitutes the receiving aperture. Several tissue and antenna properties caused us to choose this design. Thermographic

studies at infrared wavelengths indicate that a considerable fraction of breast cancer tumors have associated temperature elevations at the skin surface.[2] We therefore expect that a still larger fraction of tumors will have associated temperature elevations within a few centimeters of the skin surface. Hence it is desirable to operate at a frequency at which the absorption coefficient of fatty tissue is low enough to permit radiation to travel several centimeters without great attenuation. At these low frequencies ($\leqslant 3$ GHz), the waveguide required to propagate radiation above the cutoff frequency becomes too large to be practical. The problem can be solved by using a waveguide filled with a low-loss, high-dielectric solid of relative dielectric constant ϵ. The required waveguide width is then reduced by a factor $\sqrt{\epsilon}$. Because of the reduction in aperture width a, there is an increase in the halfwidth of the antenna power pattern in the far field, $\sim\lambda$(in fat)/a. The near-field pattern, however, will have a linear width only slightly greater than a. Hence if the hot region is located in the antenna near field, the reduction in aperture size because of dielectric filling yields an antenna of more practical size and superior spatial resolution. A lower limit on the aperture width is imposed by the requirement that the near field extend a significant distance into the tissue. The distance which divides the near and far fields may be estimated by $2a^2/\lambda$ (in fat). For an operating frequency of 3 GHz and an aperture width of 2.3 cm, the extent of the near field into the fat is then 2.4 cm.

In addition to optimizing the angular response of the antenna, it is necessary to minimize losses from impedance mismatch between the tissue and the antenna. The impedance of the fat is Z(free space)/$\sqrt{\epsilon(\text{fat})}$, or $\sim$170 Ω. The skin impedance is considerably lower, but at frequencies below 3 GHz the skin thickness of $\sim$2 mm is a small fraction of a wavelength. Hence the effect of the skin layer is negligible as far as reflections are concerned. Introduction of a 377 Ω air gap of size comparable to a wavelength between the antenna and the tissue can, however, cause a significant decrease in received power. Therefore it has proved best to place the antenna flush against the skin, with no intervening air gap. The TE mode impedance inside the dielectric-filled waveguide cannot be compared directly with the tissue impedance for matching purposes, since mode transformation occurs at the tissue-waveguide interface. Instead, VSWR measurements have been carried out to determine the frequency range over which the VSWR at the interface is smallest. Our measurements indicate that the impedance of the antenna-tissue combination as a function of frequency is dominated by cavity resonances. In effect, the dielectric-filled waveguide acts as a cavity resonator with one weakly reflecting wall. VSWR measurements of several trial antennas have thus facilitated choice of frequency bands in which reflections are minimized. Further measurements of this kind will be made as new trial antennas are constructed.

Measurements of antenna power patterns have also been made, and more are in progress. In order to determine the antenna pattern in fatty tissue, several plastic phantom

models of fat have been prepared. The plastic was mixed in accord with the recipe given by Guy and Lehmann.[7] The real and imaginary parts of the simulator dielectric constant were measured at 1 GHz and 3 GHz. They agree within 5% with measured values for human fat.[4] We have also measured E plane and H plane patterns at 3.2 GHz in the far field. Near-field measurements are in progress at this and other frequencies. In the pattern-measurement technique a dielectric-filled waveguide is used for both transmitting and receiving antennas, and it is similar to that used by Richmond and Tice.[8]

We expect to continue work now under way in two areas: development and testing of a 1-GHz radiometer; and radiometric measurements of artificially heated animal tissue. The selection of components for a radiometer to operate at 1 GHz is nearly complete. Most components are now on order. Several trial antennas have been designed and are under construction. Dielectric inserts have been fabricated, including one set of TiO_2 inserts with $\epsilon = 85$. This insert permits a reduction in waveguide aperture size by a factor of 9.2.

Plans for radiometric measurements of heated areas of live animal tissue have been developed in consultation with Professor P. P. Lele, of the Laboratory of Experimental Medicine, and with Dr. K. Goddard, of the Department of Nutrition and Food Science, M. I. T. Our goal is to heat a region of tissue in a laboratory animal by a few degrees Kelvin, over a volume comparable to the region of elevated temperature surrounding a typical breast cancer tumor (a few cm^3). The initial method of heating employs focused ultrasound.[9] Future methods may involve creation of an abscess, or actual tumor implantation. The distribution of temperature in the tissue is monitored by several implanted thermocouples. The radiometric response is then measured as a function of frequency, time, depth of the hot region beneath the skin surface, size of the hot region, and other appropriate variables. Initial measurements of this type were conducted, in August 1972, on the thigh muscles of dead and live cats. The measurements indicate microwave detection of hot spots ~1-3 cm^3, with peak internal temperatures 3-8°C above ambient.

A. H. Barrett, P. C. Myers

References

1. R. B. Barnes, Science 140, 870 (1963).
2. J. Gershon-Cohen, M. B. Hermel, and M. G. Murdock, Cancer 26, 1154 (1970).
3. T. S. England, Nature 166, 480 (1950).
4. H. P. Schwan and K. Li, Proc. IRE 44, 1572 (1956).
5. J. R. Mallard and D. G. Lawn, Nature 213, 28 (1967).
6. S. J. Webb and A. D. Booth, Science 174, 72 (1971).
7. A. W. Guy and J. F. Lehmann, IEEE Trans., Vol. BME-13, p. 76, 1966.
8. J. H. Richmond and T. E. Tice, IRE Trans., Vol. MTT-3, p. 32, 1965.
9. P. P. Lele, J. Physiol. 160, 494 (1962).

C. CENTIMETER-WAVELENGTH INTERFEROMETER-APERTURE SYNTHESIS FACILITY

We are continuing construction of a three-element centimeter-wavelength interfer-ometer.[1] The interferometer is on a 1000-ft East-West baseline, with two fixed antennas 500 ft apart and a third antenna that can be moved along a 500-ft section of railway track. A NOVA 800 computer will be used for antenna control and on-line data processing.

1. Site

The site selected for the facility is at the Haystack Observatory, Westwood, Massa-chusetts, where access roads, power, and workshops are already available. This site will permit joint observations between the interferometer and the Haystack 120-ft radio telescope. The site just south of the Haystack facility has been cleared, an access road has been built, and construction of footings and foundation pads for antennas and rails is under way.

2. Antennas

Three 18-ft reflectors have been fabricated from fiber glass and covered with a .005 in. zinc reflecting surface. All of the antennas have measured rms deviations from a best-fit parabola of approximately .012 in. The back-up structure is of alumi-num. The altazimuth mounting platforms are ready for erection at the site. Auxiliary hardware, such as motors, drive-gear trains, and so forth, has been designed and is on hand or on order.

3. Receiver System

Initially, we shall use the receiver systems developed for the 2-cm interferometer by Papadopoulos and Burke.[2] The system will use crystal mixers with a phase-lock

system that incorporates a modulated laser beam.

4. Computer System

The NOVA 800 computer is on hand, and programs are being written. Some are being adapted from those developed for the 2-cm interferometer system.

B. F. Burke, R. M. Price, G. D. Papadopoulos

P. C. Crane, D. C. Papa, J. W. Barrett

References

1. A. H. Barrett and B. F. Burke, "Aperture Synthesis," Quarterly Progress Report No. 104, Research Laboratory of Electronics, M. I. T., January 15, 1972, p. 73.

2. G. D. Papadopoulos and B. F. Burke, "Millimeter-Wave Interferometer," Quarterly Progress Report No. 106, Research Laboratory of Electronics, M. I. T., July 15, 1972, p. 5.

D. APERTURE SYNTHESIS OF EXTRAGALACTIC OBJECTS

1. Introduction

During the past year observations have been made of galaxies M31, M33, and M51 at 3.7 cm and 11.1 cm using the NRAO three-element interferometer. Full aperture-synthesis maps have been made of M31 and M33 and are being studied. Only a partial synthesis map of M51 is now available.

In this report we discuss the results obtained for each galaxy.

2. Structure of Small Sources in M51

High-resolution maps of 21-cm continuum radiation from M51 (NGC 5194/95) have recently been prepared by Mathewson, van der Kruit, and Brouw[1] from observations made with the Westerbork Synthesis Radio Telescope. We have made observations at 11.1 cm to determine the flux, polarization, and structure of 5 discrete sources shown in these maps. The only interferometer configuration that has been used thus far furnished maximum spacings of 17,100, 13,500, and 3600 wavelengths. Fourier conversion of the corrected crosscorrelation functions yielded the continuum map shown in Fig. III-6. The primary antenna pattern is shown in the lower right-hand corner. The more distant sidelobes of the pattern, which can be strong, are not shown, but are reflected in the data. The characteristic size of the largest observable feature is also indicated; it is an ellipse approximately 60" × 90". This limit is the result of the lack of short interferometer spacings in the observing program.

The map shown in Fig. III-6 is centered on HII region No. 51, and since the map has not been corrected for the primary antenna pattern, the sensitivity at the edge of the map

is only 0. 85 the sensitivity at the center of the field. Westerbork positions are indicated by crosses, and very good positional agreement is found for 4 of the sources. The source identified[1] as HII region No. 53/55 is confused with sidelobes on our map. In this report we present data on the other sources, the suggested supernova remnant iden- tified by Mathewson, et al., as HII region No. 51, the nearby source described as Source 1, and the nuclei of NGC 5194 and NGC 5195, although NGC 5195 is outside the field of view of Fig. III-6.

Our results are summarized in Table III-2. The flux uncertainty was estimated from knowledge of the system noise. In the case of complex sources, allowance was made for uncertainty in source structure. The spectral indices were determined from the flux densities of Mathewson, et al.,[1] and the work reported here.

The nuclear region of M51 is partially resolved into an elongated central complex 10" $\times$ 20" with a principal extension North-South close to the major axis of the galaxy. If we adopt 4 Mpc as the distance to M51, following Roberts and Warren,[2] and if the inclination of the plane of the galaxy to the plane of the sky is assumed to be 35°, it gives linear dimensions of 240 $\times$ 400 pc. These dimensions are entirely comparable to those of the structure in the center of our own galaxy. More structure is present in the vicin- ity of the central complex, but a precise description cannot be given until there is a more complete synthesis, since there are confusion effects from close-in sidelobes. We may certainly conclude, however, that there is a source, or a complex of sources, 18" from the optical nucleus at position angle 290°. The impression is that the nucleus is active, with no tendency toward disklike symmetry; rather, it may be composed of discrete active subregions.

The nucleus of the comparison source NGC 5195 is outside the field of Fig. III-6, but we have observations that show a region of complex structure, and the position of the radio nucleus[1] at 21 cm coincides with a weak point source. Within 15" to the south, however, other sources of greater intensity were detected, and it is clear that we need a more complete synthesis before a clear picture can be obtained. The flux of the total region is 4-6 times that of the source given in Table III-2.

The point source identified[1] as HII region No. 51, and suggested by Mathewson et al. to be a remnant of a supernova, is effectively a point source on our map. The small size and the steep spectral index of 1. 5 indicate that this is indeed a relatively young supernova remnant of the same class as Cas A. The recent observations of the 5C3 sources by van der Kruit[3] show, however, that sources of steep spectral index (steeper than 1. 0) are scattered randomly about the field with no tendency to lie within the optical image of M31, and are therefore extragalactic. This may possibly be an argument for the extragalactic nature of the source on our map, but the coincidence of this source with the emission nebula makes it much less probable that it is a projection effect than that it is a supernova remnant. A recent study of the spectrum of Cas A by Baars and
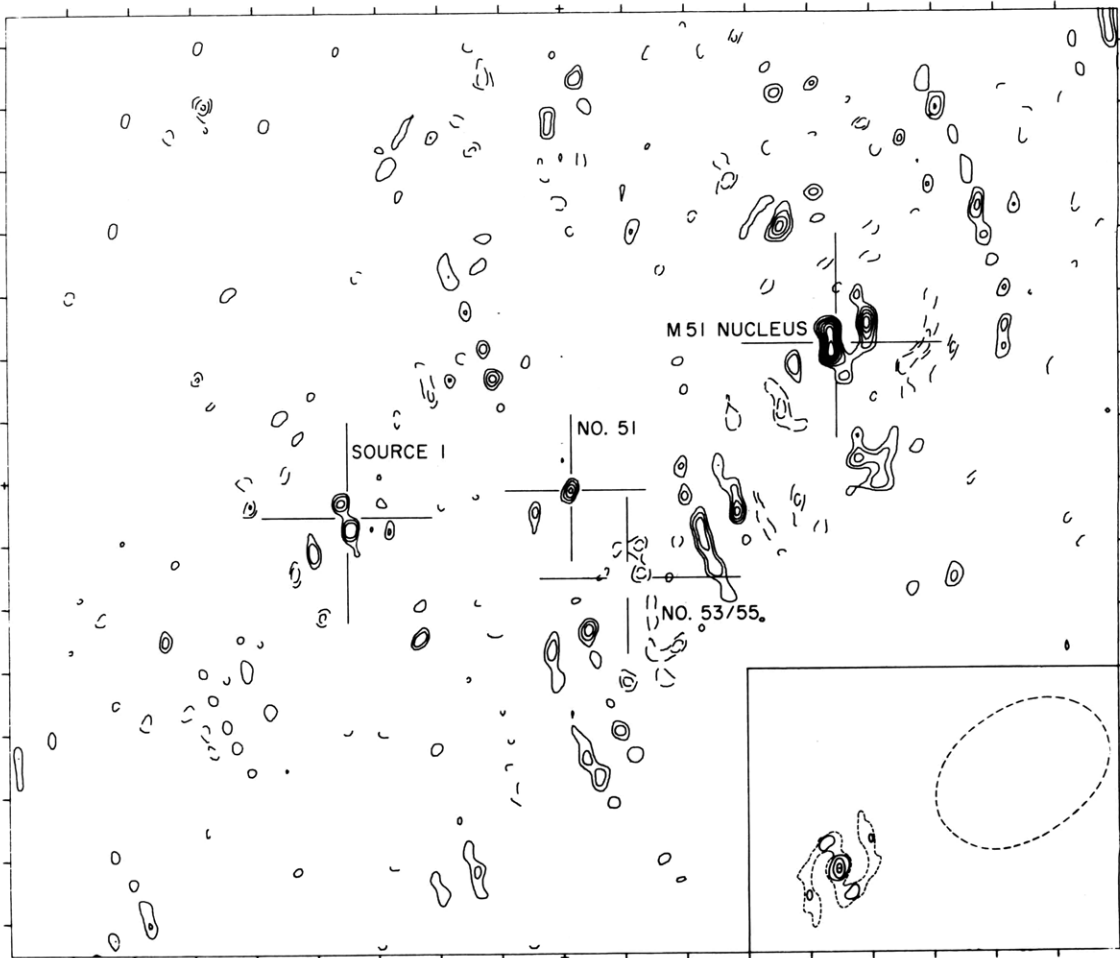
Fig. III-6. Synthesized map of a region of M51, centered on H II No. 51 region. Crosses indicate the Westerbork positions. Inset: Antenna pattern. Structures with a scale larger than the ellipse will not give a response. Field of view: R.A. 9 min of arc and Dec. 7.5 min of arc.

Table III-2. Discrete sources studied in M51.

Source	Flux	Spectral Index	Notes
NGC 5194 Nucleus total	51±8	0.7	
Central Complex	38±5		Elongated 20" NS, 10" EW
West Component	13^{+3}_{-6}		Confused by sidelobes of the central complex
NGC 5195 Nucleus	6±3	—	Source at optical position only
H II No. 51 (SNR?)	7±1	1.5	
H II No. 53/55	—		Confused by sidelobes of the M51 nucleus
Source 1 total	16±3	.63	Double, Separation 15"
North Component	6±3		
South Component	10±2		

Hartsuijker[4] presents evidence for a change in the spectral index with time, with the steep spectral index possibly characteristic of a very young supernova remnant. Their quantitative numbers, however, are not convincing. It would take approximately 400 years with their numbers for a 1.5 spectral index to become flattened to 0.8, the present value for the Cas A spectral index, and this would take more time than the age of Cas A. Alternatively, in the discussion by Mathewson et al. N49, the supernova remnant in the Large Magellanic Cloud, is used as a prototype to argue that it appears quite reasonable from the point of view of radio luminosity for this source to be a supernova remnant.

The radio source designated H II region No. 53/55 is confused by the sidelobes of other sources, and cannot be studied from this set of data.

The background object, Source 1, shows as a double source with a nonthermal spectrum. There is no optical counterpart, but the small separation and weak flux imply that this is a radio galaxy of Cyg A type that is much too distant to be observed optically.

3. Selected Fields of M31

The large angular size of M31 (NGC 224) made it necessary to observe only 5 selected fields of the galaxy. These five fields were selected within 70 min of arc (~14 kpc) of the nucleus and are centered on H II regions identified by Baade and Arp.[5] Each field is the size of the 85-ft antenna principal beam of the interferometer, which is 18 min of arc at 11.1 cm and 6 min of arc at 3.7 cm. Nineteen other fields were sampled to determine how normal the five fields that were studied in depth are. These additional fields were observed only in one configuration of the interferometer (3 baselines) and usually had detection limits of 3-4 m.f.u. (1 m.f.u. = 10^{-29} W m^{-2} Hz^{-1}).

Four of the five fields contain sources from the 5C3 catalog of Pooley.[6] Three of these show sources of 15 m.f.u. or stronger. In the nuclear field there are no sources within 30 sec of arc of the nucleus with a flux greater than 4 m.f.u. This is not what would be expected from a consideration of the lower frequency observations of Pooley[6] and of van der Kruit.[3] The fifth field contains no 5C3 sources but several H II regions. The maps have many sources at low flux levels.

4. Aperture Synthesis of M33

The Sc galaxy M33 (NGC 598) is mapped in 5 fields which completely cover the optical image of the galaxy at 11.1 cm. The coverage at 3.7 cm is not complete because of the smaller size of each field. With a field centered on NGC 604 this H II region has been mapped at both frequencies. It is a region dominated by two extended sources. In contrast, the H II region NGC 595 appears on the maps almost as a point source. A strong point source appears in a field northwest of NGC 595 and is probably not associated with M33. The three fields centered on the nucleus, the southern spiral arm, and one to the

west contain many faint sources which will take considerable time to analyze.

5. Conclusions

Based on the present maps, we conclude that M31, M33, and M51 are very different from each other, and possibly from our galaxy. M31, an Sb galaxy, has long been compared with the Milky Way. Many important studies are based on the assumption that the constituent parts of M31 are similar to the components of our galaxy. Our maps show, however, that at 11.1 cm and 3.7 cm the HII regions of M31 do not have the radio continuum of the HII regions in our galaxy. They are much fainter. Furthermore, the nucleus does not have a strong point source as does the nucleus of the Milky Way.

The small Sc galaxy M33 seems to have HII regions that have radio continua more like the HII regions in our galaxy, but it too does not have a radio nucleus similar to the galactic center. This may be a result of its smaller size and mass, because the third galaxy studied, M51, which is also an Sc galaxy but larger, has a complex radio center very similar to our galactic center. It is too distant for us to expect to detect radio continua from individual HII regions, and we do not. This, then, is only an upper limit.

J. H. Spencer, B. F. Burke

References

1. D. G. Mathewson, P. C. van der Kruit, and W. N. Brouw, Astron. Astrophys. 17, 468 (1972).
2. M. S. Roberts and J. L. Warren, Astron. Astrophys. 6, 165 (1970).
3. P. C. van der Kruit, Astrophys. Letters (in press).
4. J. W. M. Baars and A. P. Hartsuijker, Astron. Astrophys. 17, 172 (1972).
5. W. Baade and H. C. Arp, Astrophys. J. 139, 1027 (1964).
6. G. G. Pooley, M. N. Roy. Astron. Soc. 144, 101 (1969).

E. RADIOMETER SYSTEM FOR GROUND-BASED MEASUREMENT OF STRATOSPHERIC TEMPERATURES

The radiometer system for ground-based measurement of stratospheric temperatures described in previous reports[1,2] is now complete. Figure III-7 shows the radiometer and phase-lock box, which are mounted in a thermally insulated tiltable box. A 10° beamwidth standard gain horn is used as the antenna. The rack containing the filter bank, A/D converter, computer for data processing, and magnetic tape recording system is shown in Fig. III-8. This rack also contains an analog synchronous detector and circuitry for the interface between the data-processing system and the radiometer.

Since the previous report,[2] the software for this system has been extended to provide text communication with the operator via the teletypewriter, and to compute rms values
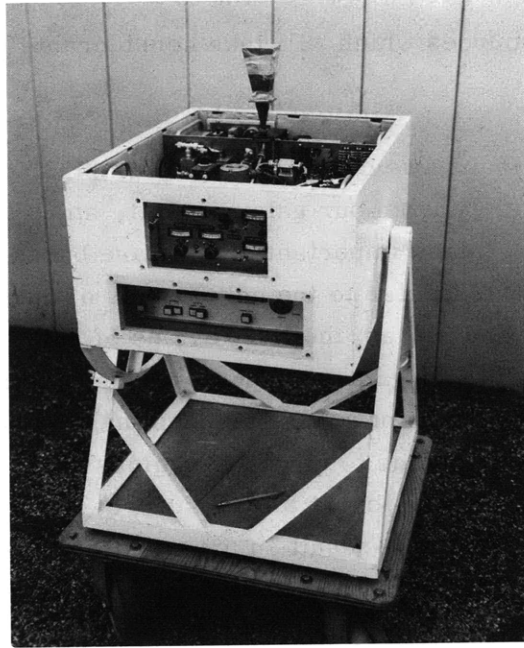
Fig. III-7. Radiometer and phase-lock box mounted in a tiltable box.
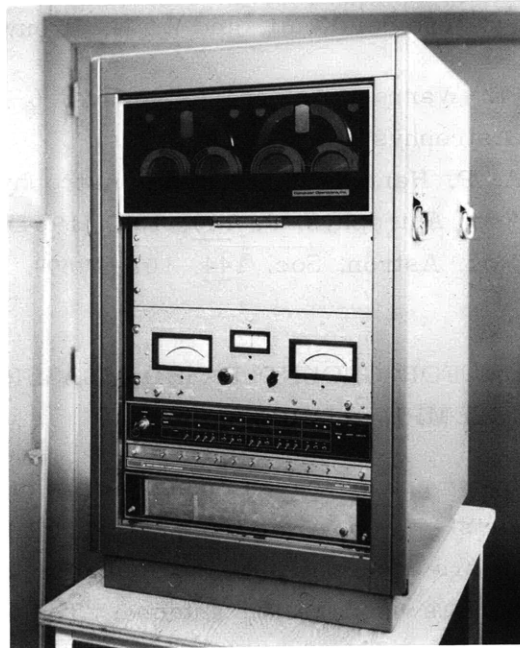

Fig. III-8. Filter bank, data processor, and magnetic tape recording system.

of the signal variations which are listed during the real-time teletypewriter output. The data-processing software has also been "interlaced" with the teletype output software, so that data taking can continue during the time (~2 min) in which a spectrum is being plotted on the teletype.

Several tests have been performed on the overall system. One of the more complete tests of the filter bank and data-processing system was accomplished by operating them in parallel with the Haystack Observatory correlator system. Results of simultaneous 4-min observations with the two systems of atmospheric emission from the 27_ O_2 line are shown in Fig. III-9 and agree within the accuracy of the measurement. Also shown
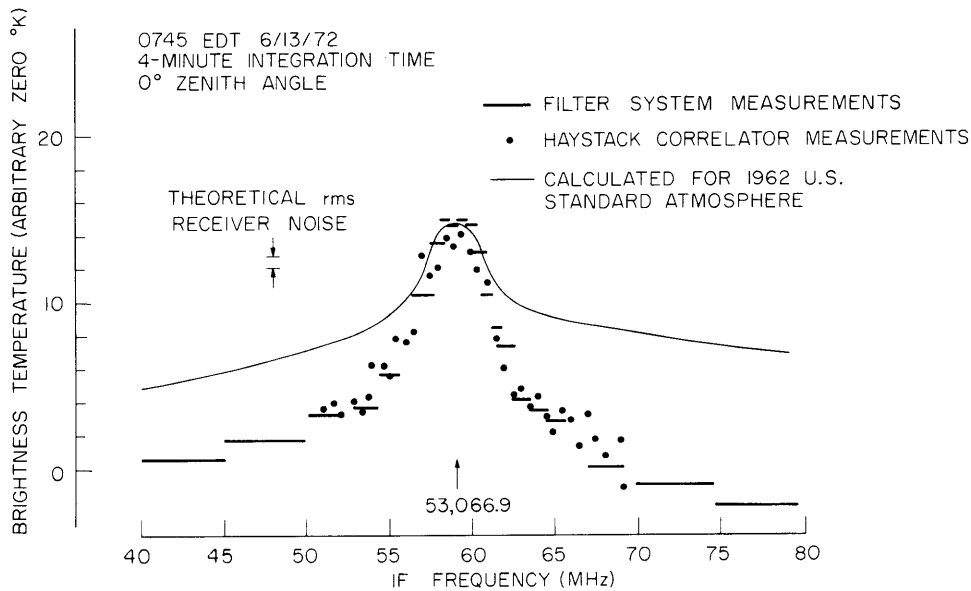

Fig. III-9. Simultaneous observations with the filter system and the Haystack correlator of atmospheric thermal emission from the 27_ O_2 line. Horizontal bars indicate filter bandwidths. The calculated emission line uses the oxygen absorption coefficient given by Barrett, et al.[3]

is the calculated emission from this line. We believe the disagreement between measurement and calculation is the result of the inadequacy of the theory which sums individual O_2 spin-rotation lines with linewidth parameters empirically adjusted by other workers to fit other measurements.

The radiometer and the filter-bank data-processing system can each be easily used with other systems. Their versatility has been demonstrated, to some extent, by the experiments described in Secs. III-F, III-G, and III-H.

<div align="right">

J. W. Waters, R. M. Paroskie, J. W. Barrett,

D. C. Papa, D. H. Staelin

</div>

References

1. J. W. Waters, J. W. Barrett, D. C. Papa, R. M. Paroskie, and D. H. Staelin, "Radiometer System for Ground-Based Measurement of Upper Atmospheric Temperatures," Quarterly Progress Report No. 104, Research Laboratory of Electronics. M. I. T., January 15, 1972, pp. 76-80.

2. R. M. Paroskie, J. W. Waters, J. W. Barrett, D. C. Papa, and D. H. Staelin, "Radiometer System for Ground-Based Measurement of Stratospheric Temperatures," Quarterly Progress Report No. 106, Research Laboratory of Electronics, M. I. T., July 15, 1972, pp. 7-8.

3. A. H. Barrett, J. W. Kuiper, and W. B. Lenoir, "Observations of Microwave Emission by Molecular Oxygen in the Terrestrial Atmosphere," J. Geophys. Res. 71, 4723 (1966).

F. GROUND-BASED OBSERVATIONS OF UPPER STRATOSPHERIC TEMPERATURE

Routine measurements of upper stratospheric temperature are now being made at M. I. T. in Cambridge by observation of the 27_ O_2 line atmospheric emission using the receiver described in Sec. III-E. Figure III-10 shows our first measurements
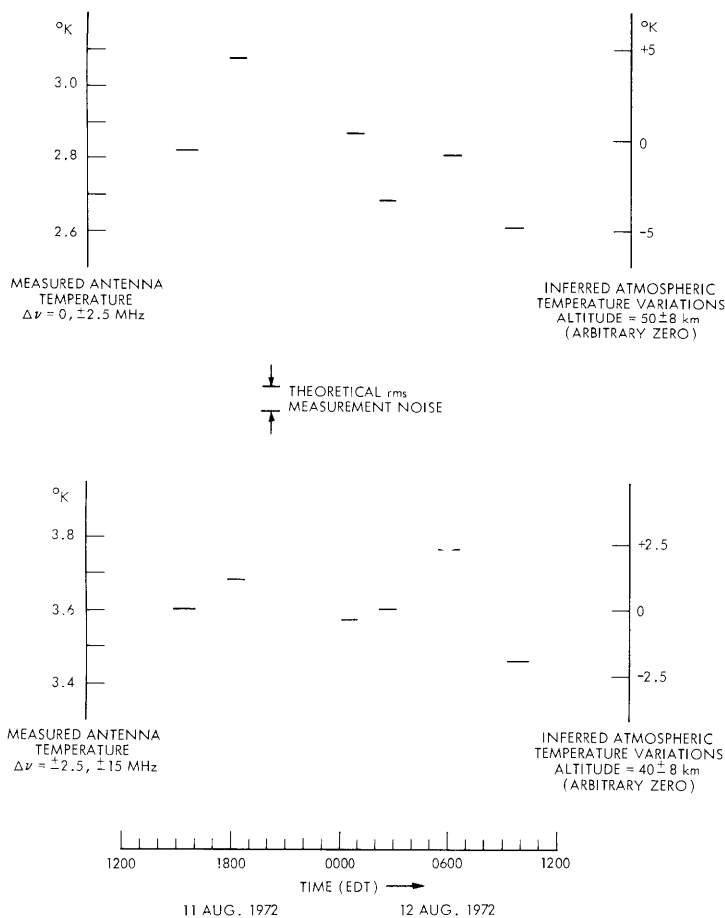

Fig. III-10.

Measured antenna temperatures and inferred stratospheric temperatures. (Zenith angle 15°.)

made during a 24-hour period on 11 and 12 August 1972. The upper portion of this figure gives the measured difference in double-sideband antenna temperature between the line center and the half-power points (±2.5 MHz from center); this difference corresponds to emission originating in the altitude region ~42-58 km. The lower portion of the figure gives the measured difference between the half-power points and the baseline (±15 MHz from center), which corresponds to radiation originating in the altitude region ~32-48 km. Atmospheric temperature variations were calculated according to a 1% change in atmospheric temperature for a 5% change in antenna temperature.

We plan to study diurnal, monthly, and seasonal variations in upper stratospheric temperatures over a period of at least one year. Until further measurements and instrument tests are made we shall not discuss the implications of the inferred temperature variations.

J. W. Waters, B. G. Anderson

References

1. J. W. Waters, "Ground-Based Microwave Spectroscopic Sensing of the Stratosphere and Mesosphere," Ph. D. Thesis, Department of Electrical Engineering, M. I. T., December 1970.

G. OBSERVATIONS OF THERMAL EMISSION FROM ATMOSPHERIC O_2 LINES

The system described in Sec. III-E has been used to measure atmospheric thermal emission from five $\Delta J = -1$ transitions on the edge of the 5-mm wavelength O_2 absorption band. Figure III-11 shows the measured emission lines. With the exception of the 27_ line which was measured earlier,[1] this is the first measurement of these lines, either in the laboratory or in the atmosphere. The frequencies[2] and relative intensities[1] are in good agreement with calculated values, but the absolute intensities disagree with calculations in the amounts shown in Sec. III-E (Fig. III-9).

High-frequency resolution measurements of the three strongest lines have also been made using the radiometer with the Haystack Observatory digital autocorrelator, and the 27_ line measurement is shown in Fig. III-12. Also shown is the calculation which linearly superimposes the 159 Zeeman components of the line spread over ±1 MHz by the terrestrial magnetic field. The calculations used the theory of Lenoir[3] with the Zhevakin-Naumov[4] line shape and linewidth parameters recently obtained by Reber.[5]
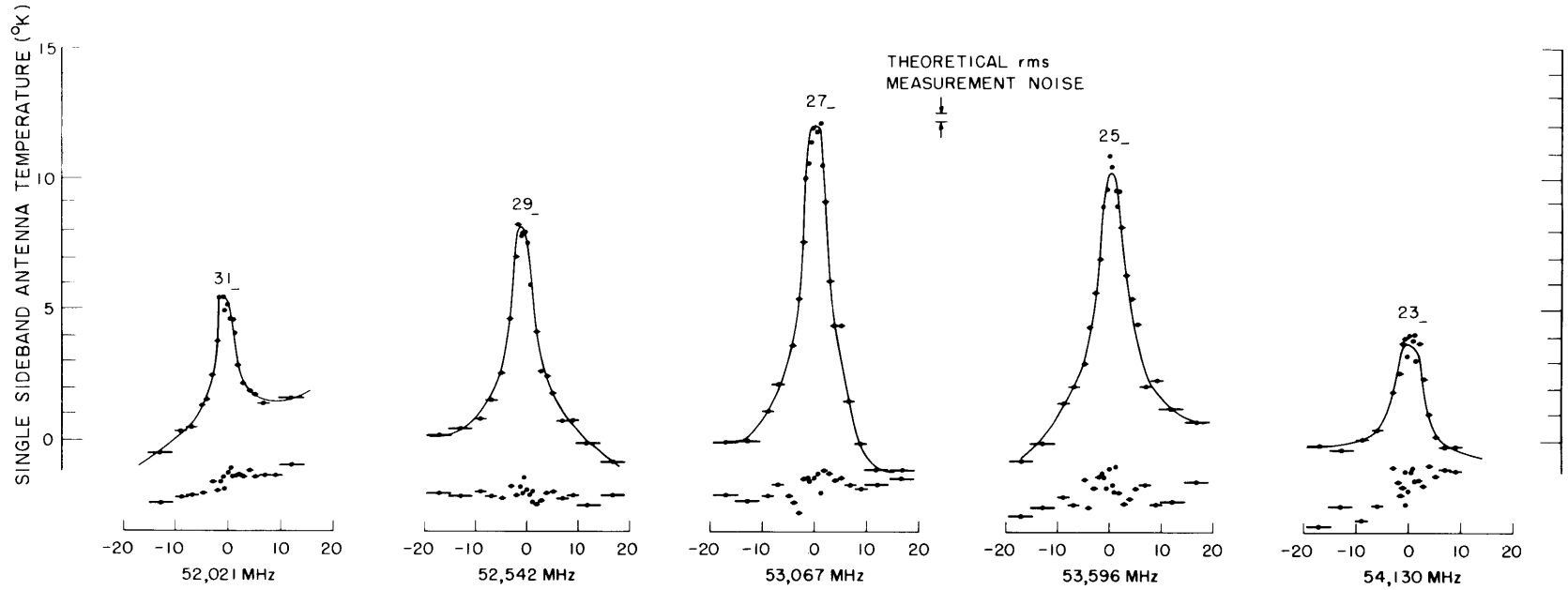
Fig. III-11.   Measured emission from atmospheric O$_2$ lines.   These measurements were made looking at the zenith during the week of August 30, 1972 at the Haystack Observatory, Westford, Massachusetts.   Below each line is the instrumental baseline which was measured by tipping the antenna to 90° zenith angle.   Each line and baseline was measured with a 15-min integration time.   The respective filter bandwidths are indicated by horizontal bars and the frequencies are those for which the filter bank was centered, not necessarily the frequency that best fits the line.   The zero level of the temperature scale is arbitrary.
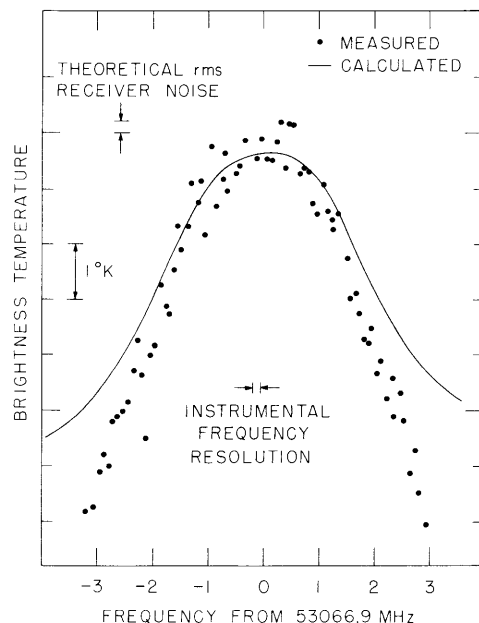
Fig. III-12.   High-frequency resolution measurement of the center of the
27_ line. The measurement was made looking at the zenith
with linear polarization. During half of the measurement
the observed electric vector was parallel to the terrestrial
magnetic field vector and during the other half these two
vectors were perpendicular.

These measurements will be discussed further in a paper that is being prepared for publication.

J. W. Waters

References

1. J. W. Waters, "Ground-Based Microwave Spectroscopic Sensing of the Stratosphere and Mesosphere," Ph. D. Thesis, Department of Electrical Engineering, M. I. T., December 1970.

2. T. T. Wilheit, Jr., "Studies of Microwave Emission and Absorption by Atmospheric Oxygen," Ph. D. Thesis, Department of Physics, M. I. T., October 1969.

3. W. B. Lenoir, "Microwave Spectrum of Molecular Oxygen in the Mesosphere," J. Geophys. Res. 73, 361 (1968).

4. C. A. Zhevakin and A. P. Naumov, "Absorption of 3 mm-7.5 mm Waves in the Earth's Atmosphere," Izvest. VUZ Radiofiz. 9, 433 (1966).

5. E. E. Reber, "Absorption of the 4- to 6-Millimeter Wavelength Band in the Atmosphere," J. Geophys. Res. 77, 3831 (1972).

H.   OZONE AND N_2O MEASUREMENTS IN THE ATMOSPHERE

A low-noise mixer at frequencies near 100 GHz has been developed for atmospheric research and radio astronomy.[1] Using this mixer, we constructed a 100-GHz radiometer
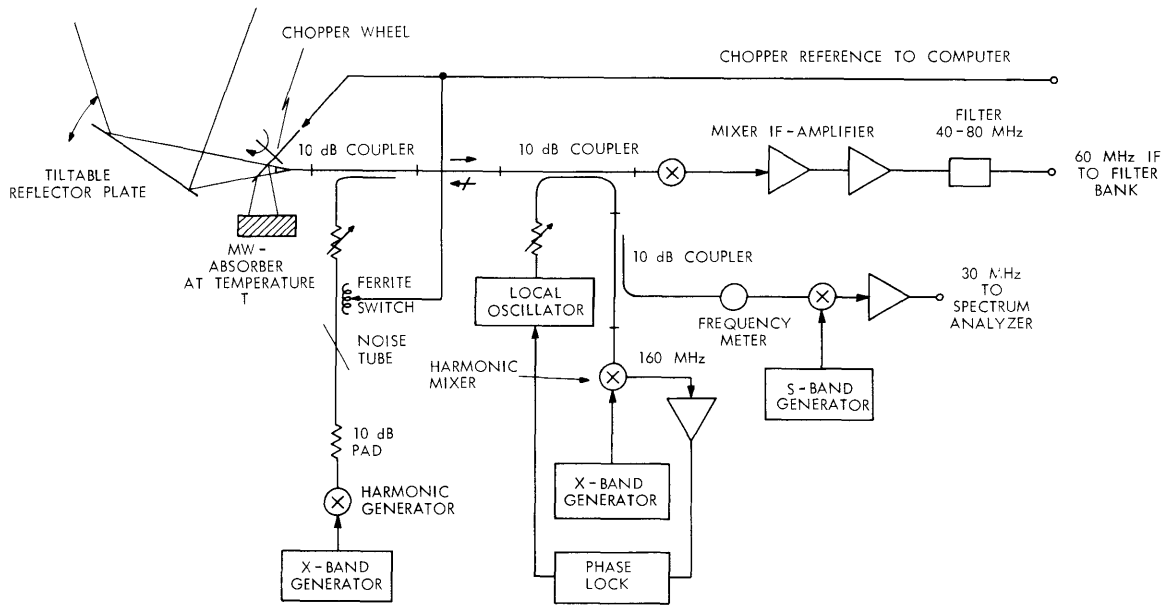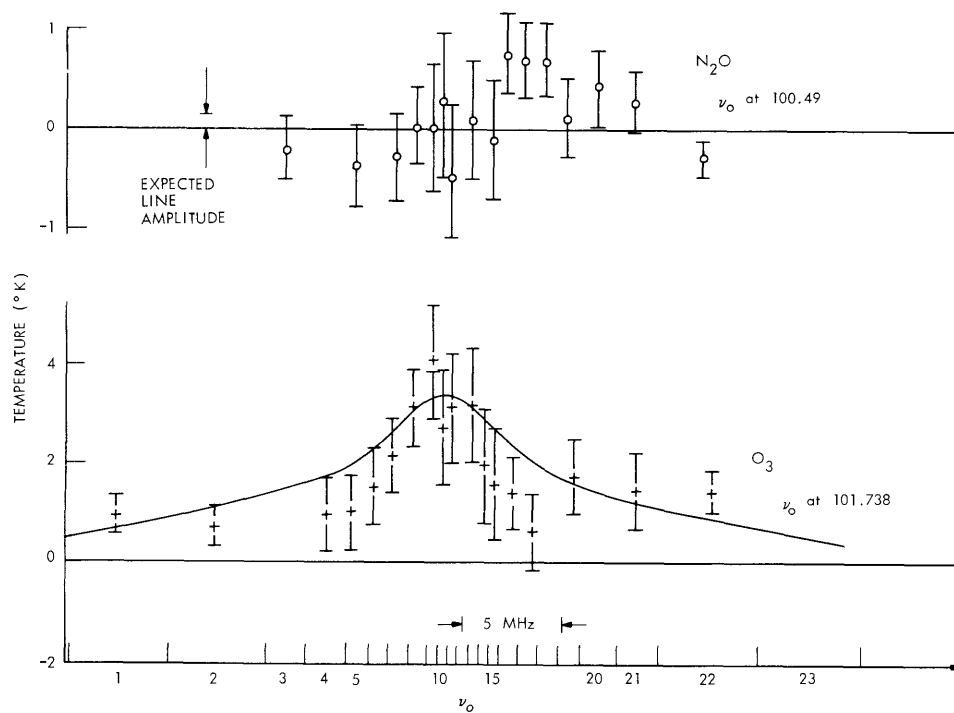
Fig. III-13. 100-GHz radiometer.

Fig. III-14. O$_3$ line at 101. 737 GHz and N$_2$O line at 100. 492 GHz. Solid line
indicates the calculated expected O$_3$ absorption line. Elevation
angle 20°. Error brackets show 2ΔT$_{rms}$.

with a double-sideband system temperature of ~5000°K. This system temperature includes 3000°K from the mixer and IF amplifier, and 2000° from insertion loss in the antenna line (mainly the isolator and the balance-noise coupler). We believe that because of the low IF (60 MHz), local-oscillator noise is still a considerable part of the total noise. Figure III-13 is a block diagram of the radiometer. The chopper wheel is used as a "Dicke switch" between the atmospheric signal and the reference signal, which is a microwave absorber at known temperature T. A reference signal from the chopper wheel is used for the synchronous detection in the computer and to drive the ferrite switch in the calibration arm. The 60-MHz intermediate frequency is fed into the filter bank. The complete back end (filter bank and computer) and the signal processing have been described previously[2] (and see also Sec. III-E). The tiltable reflector plate in front of the antenna permits different observing angles. The local-oscillator klystron was phase-locked to the 10th harmonic of an X-band klystron stabilized to a crystal oscillator. The stability achieved was better than 10^7. The local-oscillator frequency was continously monitored by observing its beat frequency with the 34th harmonic of a stable S-band oscillator. Initially, for each measurement the radiometer frequency was checked by observing the 10th harmonic of a stabilized X-band klystron (Marker) simulating the line under consideration.

Figure III-14 shows an example of the observed O_3 line at 101.737 GHz. The solid curve is a theoretical calculation made by J. E. Rudzki.[3] The measurements were terminated because of failure of the local-oscillator klystron.

We also tried unsuccessfully to measure the expected line of N_2O at 100.492 GHz with a calculated amplitude of approximately 0.3°K. These calculations[4] are very uncertain because the absorption coefficients are not well known. Therefore, the expected line amplitude can be considerably larger or smaller than indicated. Our measurement gives an upper limit (1 standard deviation for the narrow-band channels) of ~0.6°K for the line.

I would like to acknowledge the help of R. M. Paroskie in programming the computer for this experiment.

K. F. Kunzi

References

1. K. F. Kunzi, "Mixer Development at 100 GHz for Atmospheric Research," Quarterly Progress Report No. 106, Research Laboratory of Electronics, M.I.T., July 15, 1972, pp. 16-17.

2. J. W. Waters, J. W. Barrett, D. C. Papa, R. M. Paroskie, and D. H. Staelin, "Radiometer System for Ground-Based Measurement of Upper Atmospheric Temperatures," Quarterly Progress Report No. 104, Research Laboratory of Electronics, M.I.T., January 15, 1972, pp. 76-80.

3. J. E. Rudzki, "Remote Sensing of Mesospheric Ozone," Ph.D. Thesis, Department of Electrical Engineering, M.I.T., January 1971.

4. J. W. Waters, "Ground-Based Sensing of Stratosphere and Mesosphere," Ph.D. Thesis, Department of Electrical Engineering, M.I.T., January 1971.